

Quantum Approximate Bayesian Optimization Algorithms with Two Mixers and Uncertainty Quantification

Jungin E. Kim¹ and Yan Wang¹

¹George W. Woodruff School of Mechanical Engineering, Georgia Institute of Technology, Atlanta, GA 30332 USA

October 23, 2023

Abstract

The searching efficiency of the quantum approximate optimization algorithm is dependent on both the classical and quantum sides of the algorithm. Recently a quantum approximate Bayesian optimization algorithm (QABOA) that includes two mixers was developed, where surrogate-based Bayesian optimization is applied to improve the sampling efficiency of the classical optimizer. A continuous-time quantum walk mixer is used to enhance exploration, and the generalized Grover mixer is also applied to improve exploitation. In this paper, an extension of QABOA is proposed to further improve its searching efficiency. The searching efficiency is enhanced through two aspects. First, two mixers, including one for exploration and the other for exploitation, are applied in an alternating fashion. Second, uncertainty of the quantum circuit is quantified with a new quantum Matérn kernel based on the kurtosis of the basis state distribution, which increases the chance of obtaining the optimum. The proposed new two-mixer QABOA's with and without uncertainty quantification are compared with three single-mixer QABOA's on five discrete and four mixed-integer problems. The results show that the proposed two-mixer QABOA with uncertainty quantification has the best performance in efficiency and consistency for five out of the nine tested problems. The results also show that QABOA with the generalized Grover mixer performs the best among the single-mixer algorithms, thereby demonstrating the benefit of exploitation and the importance of dynamic exploration-exploitation balance in improving searching efficiency.

1. Introduction

Quantum computers are promising in solving large-scale engineering problems such as optimization [1]-[2] and simulation [3]-[4]. However, the capability of current quantum computers to solve large-scale problems is limited. One reason is that the number of qubits on current quantum computers is small, whereas many qubits are required to represent the large searching space as the number of variables increases. Another reason is that decoherence can occur easily on quantum computers due to environmental noise, which makes useable quantum computing time very short.

One optimization algorithm that was recently developed for noisy intermediate-scale quantum computers is the quantum approximate optimization algorithm (QAOA) [5]. The goal of QAOA is to find optimal rotation angles for a quantum circuit to increase the amplitude of the optimal basis state. The circuit consists of phase-separating and mixer Hamiltonian operators in an alternating fashion. The phase-separating Hamiltonian operator encodes the objective quantity being optimized, whereas the mixer Hamiltonian operator alters the basis state amplitudes. By incorporating a classical optimization algorithm to optimize the rotation angles, this hybrid quantum-classical algorithm can alleviate the decoherence issue.

QAOA is a heuristic optimization algorithm. Its searching efficiency is dependent on both the classical and quantum sides of the algorithm. Several approaches have been proposed to improve the efficiency of QAOA. One approach is to customize the quantum circuit based on the problem. By taking advantage of functional relationships between the objective quantities and the quantum circuit parameters [6]-[7], or exploiting the symmetry of the objective function [8], the size of the rotation angle searching space is reduced. Another approach is to initialize the quantum circuit other than the uniform superposition. Examples of initialization strategies are warm-start preprocessing [9] and Dicke states [10], which are based on the prior knowledge about the potential solutions. A third approach is to define the phase-separating Hamiltonian with an Ising model of higher order than the quadratic form [11]. This binary native encoding scheme can achieve higher quality solutions than the unary and binary reduced encoding schemes.

The most critical component of QAOA is the mixer operator, which determines how the state of the quantum system evolves. Several mixers have been proposed to improve the searching efficiency of QAOA. Some mixers such as the XY mixer [12]-[13] and the continuous-time quantum walk mixer [14] restrict the search space to the states which satisfy problem constraints. The generalized Grover mixer [15] increases the amplitudes of basis states associated with improved objective values. The continuous-time quantum walk and generalized Grover mixers are also combined to improve the exploration-exploitation balance [16]. A free-axis mixer [17] and an entangled gate mixer [18] induce a wider exploration of the basis states.

Since mixers affect the searching efficiency of QAOA, the design of mixers should incorporate the exploration-exploitation balance. Exploration involves finding the global optimal solutions in new regions of the search space, whereas exploitation involves further improving the current best solution locally. Maintaining a good balance between exploration and exploitation is important for high searching efficiency. Over-exploration may miss the opportunity to further improve the solution, whereas over-exploitation has the risk of being trapped at a local optimum.

One way to achieve the exploration-exploitation balance is to incorporate two mixers in the quantum circuit. The first mixer emphasizes exploration by altering the basis state amplitudes. The second mixer performs exploitation by increasing the amplitudes of better solutions. In the recent quantum approximate Bayesian optimization algorithm (QABOA) [16], the continuous-time quantum walk mixer enhances exploration, whereas the generalized Grover mixer improves exploitation. This two-mixer design can effectively improve the balance. In addition, Bayesian optimization (BO) is utilized in QABOA for the classical optimization side. BO is a surrogate-based global optimization approach that can improve the sampling efficiency of optimization. Gaussian process regression (GPR) model is the most commonly used surrogate for sequential sampling in BO. An acquisition function is constructed based on the surrogate to guide the search into the most promising regions. The acquisition function can also be designed to achieve a good exploration-exploitation balance.

The above research efforts are to improve the searching efficiency of the QAOA. The uncertainty associated with quantum circuit evaluation and quantum noise, however, was not considered. The probabilistic nature of measurements leads to non-deterministic and random results. The quantum noise is due to the errors and decoherence of the computer system. Incorporating uncertainty is important to improve consistency and speed of convergence.

In this work, an extension of QABOA is proposed to further improve its performance. The searching efficiency is improved through two aspects. First, two mixers, including one for exploration and the other for exploitation, are applied in an alternating fashion. Pauli-X, XY, and quantum walk are examples of exploration mixers. The generalized Grover mixer is for exploitation through amplitude amplification. The new algorithm with two mixers is referred to as TM-QABOA. TM-QABOA can be used to solve both discrete and mixed-integer optimization problems, where BO is performed to optimize both rotation angles and continuous variables in the original objective function. Second, uncertainty of the quantum circuit is incorporated in the searching. The uncertainty is quantified by introducing a new quantum Matérn kernel based on the estimated kurtosis, or peak sharpness, of the basis state distribution. The version of TM-QABOA which incorporates the uncertainty is referred to as uTM-QABOA. The results of uTM-QABOA show that the searching efficiency can be improved with the consideration of uncertainty. The number of quantum circuit runs in the proposed QABOA's is reduced in two aspects. First, an improved exploration-

exploitation balance with the two mixers can help obtain the optimal solution faster. Second, surrogate-based BO can reduce the number of objective function evaluations which correspond to the quantum circuit runs.

The remainder of the paper is structured as follows. In Section 2, the relevant work of improving QAOA efficiency is reviewed. The sources of uncertainty in quantum optimization algorithms and the methods to reduce quantum noise are introduced. The proposed TM-QABOA methodology is described in Section 3. In Section 4, the TM-QABOA is demonstrated and evaluated with nine optimization problems. The problems include a MaxCut problem, three weighted MaxCut problems, lattice protein folding, HeH⁺ potential energy minimization, as well as the designs of a welded beam, a speed reducer, and a pressure vessel. The first five are discrete optimization problems, whereas the last four are mixed-integer problems. Future extensions of TM-QABOA are discussed in Section 5.

2. Relevant Work

2.1. Existing Mixers to Improve the QAOA Efficiency

The goal of QAOA is to optimize rotation angles for the quantum circuit to increase the optimal basis state amplitude. Given an n -qubit quantum system, the QAOA quantum circuit with a depth of p is defined as

$$|\psi\rangle = U_B(B, \beta_p)U_C(C, \gamma_p) \cdots U_B(B, \beta_1)U_C(C, \gamma_1)|+\rangle^{\otimes n} \quad (1)$$

where $|+\rangle^{\otimes n}$ is the initial state of the n -qubit system with uniform superposition. $|\psi\rangle$ is the final state. The operator $U_C(C, \gamma)$ is the phase-separating Hamiltonian operator with phase-separating Hamiltonian C and rotation angle γ . The mixer operator $U_B(B, \beta)$ is defined with mixer Hamiltonian B and rotation angle β . The quantum circuit alternates between U_C and U_B for p repetitions. The operator U_C encodes the objective quantity being optimized, whereas U_B perturbs the quantum system to change the system's state.

The choice of B affects how the quantum system evolves. Various mixers have been proposed to improve the QAOA searching efficiency. One type of mixer is the XY mixer [13], which explores basis states that are topologically connected as graphs. With this graph structure, the XY mixer ensures that only feasible states are explored. XY mixers are used in the quantum alternating operator ansatz [12], which results in a faster search process than the original QAOA with Pauli-X mixers. The two mixers have been compared in solving different problems, such as k-vertex cover [10], portfolio optimization [19], and extractive text summarization [20]. Furthermore, the phase-separating and XY mixer operators are combined into a two-parameter unitary operator [21]. As a result, the quantum circuit depth is reduced. Another mixer is the continuous-time quantum walk [14]. This mixer is similar to the XY mixer by which it represents

the feasible basis state space in combinatorial problems as graphs. With this mixer, the quantum system’s evolution follows the problem constraints.

The generalized Grover mixer [15]-[16] is based on Grover’s algorithm [22] originally developed for the unstructured database search problem. In the generalized Grover operator, a rotation parameter is introduced which replaces the fixed π rotation angle. The generalized Grover operator can be used as a mixer in QAOA. Recently, Wang [16] proposed QABOA. The quantum circuit consists of the generalized Grover operator and the continuous-time quantum walk as two mixers which are applied together. BO is applied to optimize the rotation angles. The QABOA quantum circuit is designed to improve the exploration-exploitation balance.

Other QAOA mixers have been devised. Govia et al. [17] proposed a free-axis mixer which performs qubit rotations about any axis in the XY plane. The mixer results in higher approximation ratios than the original QAOA. Chen et al. [18] incorporated quantum entanglement of Pauli-X and Pauli-Y mixers to improve convergence. Similarly, Yu et al. [23] proposed the adaptive bias mixer which combines the Pauli-X and parameterized Pauli-Z gates to reduce the circuit depth. Chancellor [24] devised a mixer which implements coupling between qubits so that the total number of qubits can be reduced.

Currently, most of the QAOA mixers either improve the searching efficiency by shrinking the search space with constraints, or improve the convergence towards the global optimum by exploring a larger search space. However, research efforts to improve the exploration-exploitation balance are limited. A dynamic exploration-exploitation balance is important to improve the searching efficiency. An algorithm which over-explores can miss the global optimum, whereas an algorithm which over-exploits can remain trapped at a local optimum. Here, an extension of QABOA is proposed to improve the exploration-exploitation balance with an alternating sequence of two mixers.

2.2. Sources of Uncertainties in Quantum Optimization

One source of the uncertainty in quantum optimization is quantum noise or computer error, which causes the state of a quantum system to change randomly. In variational algorithms such as QAOA, quantum noise results in the rotation angles deviating from optimal values [25]-[26]. A common approach to reduce quantum noise is quantum error correction [27], where the state of the quantum system is encoded with a redundant number of qubits. Examples of quantum error correction algorithms include Shor’s method [28], stabilizer codes [29], surface codes [30]-[31], and bosonic codes [32]. Another approach is to implement a noise model which captures noise. For example, an extension of the variational quantum eigensolver was proposed [33], where a GPR model is applied to reduce noises in objective values. With the GPR, the number of iterations to find near-optimal solutions decreases.

Another source is the non-deterministic nature of basis state measurements. Given the same rotation angles in the QAOA circuit, obtaining the same optimal solution from multiple runs is not guaranteed. To improve the consistency and speed of convergence, the random error associated with the amplitude estimation for the optimal solution needs to be estimated.

In general, when measurements are taken, the uncertainty associated with the amplitudes is the combined effect from both computer error and random error. The quantification of the uncertainty associated with the amplitudes is currently unexplored in QAOA's. In this work, a method of quantifying the uncertainty is proposed.

3. Proposed Quantum Approximate Bayesian Optimization Algorithms with Two Mixers (TM-QABOA)

In this section, the proposed TM-QABOA methodology is described. In TM-QABOA, BO is combined with a quantum circuit consisting of three types of unitary operators arranged in an alternating fashion. FIGURE 1 illustrates the TM-QABOA architecture, where BO is the outer optimization loop, and the quantum circuit is the inner one. The three types of unitary operators include phase-separating Hamiltonian operators U_C 's, mixer Hamiltonian operators U_B 's, and generalized Grover mixers U_G 's. First, each U_C is associated with a rotation angle γ_i ($i = 1, \dots, p$) and phase-separating Hamiltonian $C(\mathbf{x}_c)$, where $C(\mathbf{x}_c)$ depends on a collection of continuous variables \mathbf{x}_c . Second, each U_B is associated with a rotation angle β_i ($i = 1, \dots, p$) and a mixer Hamiltonian B . Lastly, each U_G is associated with a rotation angle θ_i ($i = 1, \dots, p$). BO is used to optimize the rotation angles. TM-QABOA can also be applied to mixer-integer optimization problems, where \mathbf{x}_c is optimized with BO. The GPR surrogate models a Gaussian distribution of possible objective values at a sample point. GPR is defined with a covariance kernel function which quantifies the similarity between solutions.

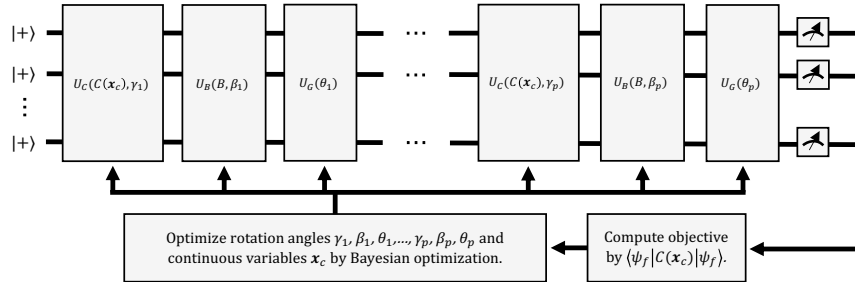


FIGURE 1. Proposed TM-QABOA architecture.

In addition, to quantify the uncertainty associated with the amplitudes of optimal solutions, a second version of TM-QABOA is proposed, referred to as uTM-QABOA. In the second version, the GPR is defined with a novel kernel function called the quantum Matérn (QM) kernel, which is the sum of the Matérn kernel and a new quantum kurtosis kernel. The quantum kurtosis kernel is inversely related to the kurtosis, or peak sharpness, of the estimated basis state distribution.

The remainder of this section is structured as follows. The quantum circuit architecture is described in Section 3.1. The BO process is described in Section 3.2. The QM kernel is formulated in Section 3.3. The procedure of uTM-QABOA is summarized in Section 3.4.

3.1. Quantum Circuit Architecture

The TM-QABOA quantum circuit with depth p is defined as

$$|\psi\rangle = U_G(\theta_p)U_B(B, \beta_p)U_C(C(\mathbf{x}_c), \gamma_p) \cdots U_G(\theta_1)U_B(B, \beta_1)U_C(C(\mathbf{x}_c), \gamma_1)|+\rangle^{\otimes n}. \quad (2)$$

The initial system state $|+\rangle^{\otimes n}$ is prepared by initializing all n qubits as $|0\rangle$ and then applying the Hadamard gate to each qubit. This results in a uniform superposition where all basis states have equal amplitudes of $2^{-n/2}$. The initial superposition is uniform since the optimal solution is unknown at first.

The first operator is U_C , which encodes the objective quantity being optimized. The operator U_C is defined as

$$U_C(C(\mathbf{x}_c), \gamma) = e^{-i\gamma C(\mathbf{x}_c)}. \quad (3)$$

Given an objective function $f(q_1, \dots, q_n, \mathbf{x}_c)$ where q_i ($i = 1, \dots, n$) is a binary variable, $C(\mathbf{x}_c)$ is computed by performing a transformation on $f(q_1, \dots, q_n, \mathbf{x}_c)$. The transformation is defined as [7]

$$q_i \rightarrow \frac{1}{2}(1 - Z_i) \quad (4)$$

where Z_i is the Pauli-Z gate acting on the i^{th} qubit.

The second operator U_B , which is the first mixer in the quantum circuit, perturbs the system from one state to another. The operator U_B is defined as

$$U_B(B, \beta) = e^{-i\beta B} \quad (5)$$

where

$$B = \sum_{i=1}^n X_i \quad (6)$$

is a collection of Pauli gates acting on all qubits. The purpose of U_B is to help explore the basis state space.

The third operator U_G , which is the second mixer in the quantum circuit, performs amplitude amplification on basis states with improved objective values. The operator U_G is a combination of two reflection operators, defined as

$$U_G(\theta) = U_R U_S(\theta) \quad (7)$$

where

$$U_S(\theta) = I - (1 - e^{i\theta}) \sum_{u \in S} |u\rangle\langle u| \quad (8)$$

shifts the phases of the target basis states by a rotation angle θ . Here, I is the identity matrix and S is the set of solutions which have better objective values than the current best objective value f^* found so far. Next,

$$U_R = U_H(I - 2|\mathbf{0}\rangle\langle\mathbf{0}|)U_H \quad (9)$$

reflects all basis states about the average amplitude. Here, $|\mathbf{0}\rangle$ is the basis state with all qubits set to $|0\rangle$ and U_H is the tensor product of n Hadamard gates.

To implement the generalized Grover mixer, two quantum registers can be utilized, similar to [34]. The first register encodes the solution of the optimization problem, while the second register is used to store the difference between the current objective value and the best solution found so far. All qubits in the second register are initialized as $|0\rangle$. The generalized Grover mixer consists of the following operations. First, Hadamard gates are applied on the second register to create a superposition of basis states. Next, several controlled gates shift the phase of each basis state by an angle proportional to the difference between the current and best objective values. The phase shifts are controlled by the first register. Third, the inverse quantum Fourier transform is applied on the second register, which converts the phase encoding of the difference between objective values into a binary representation. As part of this representation, one of the qubits in the second register indicates the sign of the difference between objective values, which helps determine the solution set S in Eq. (8). Next, the phases of target basis states are shifted by an angle θ . This operation is controlled by the qubit representing the sign of the value difference. After the phases of the target basis states are shifted with U_S , U_R is performed on the

first register. The second register is then uncomputed to reset the qubits to $|0\rangle$ in order to release the register entanglement.

After repeating the sequence of U_C , U_B , and U_G for p times, the measurement operators collapse $|\psi\rangle$ into a single basis state $|\psi_f\rangle$, which is the optimal solution that the algorithm identifies. The objective value corresponding to $|\psi_f\rangle$ is computed from the expectation of $C(\mathbf{x}_c)$, defined as

$$f(\mathbf{x}_c, |\psi_f\rangle) \approx \langle \psi_f | C(\mathbf{x}_c) | \psi_f \rangle. \quad (10)$$

The TM-QABOA quantum circuit is designed with two mixers to improve the searching efficiency by inducing a dynamic exploration-exploitation balance. The first mixer U_B alters the basis state amplitudes for exploration of different basis states, whereas the second mixer U_G helps exploit basis states with improved objective values. Alternating between both mixers can potentially increase convergence towards optimality by which basis states with improved objective values are more likely to be measured.

3.2. Bayesian Optimization

In the proposed TM-QABOA framework, surrogate-based BO is used to optimize the quantum circuit rotation angles $\gamma_i, \beta_i, \theta_i$ ($i = 1, \dots, p$), and the continuous variables \mathbf{x}_c in the original objective function. In contrast to gradient-based local optimization methods, BO is a surrogate-based global optimization approach. It does not require the objective function to be explicitly known. A surrogate of the objective function is constructed to improve the searching efficiency. BO does not require the derivatives of the objective function to be computed. The number of objective function evaluations can be significantly reduced. Furthermore, uncertainty of the objective is incorporated into the GPR surrogate model so that the robustness of the optimization is improved. Here, the uncertainty associated with quantum computation is quantified based on BO by defining a new QM kernel.

In BO, the GPR surrogate model is trained and updated on a collection of sample points. The GPR generates a distribution of possible objective functions which fit the known sample points. The mean and standard deviation of the surrogate model are used to determine another sample point to add to the collection. The selected sample points guide the search process towards the optimal solution.

First, an initial collection of sample points are obtained from either a pre-existing dataset or random sampling from the search space. The GPR is then constructed based on the sample points. Given a sample point \mathbf{x} in the search space, the objective value $f(\mathbf{x})$ follows a Gaussian distribution, defined as

$$f(\mathbf{x}) \sim GP(m(\mathbf{x}), K(\mathbf{x}, \mathbf{x}')) \quad (11)$$

where $m(\mathbf{x})$ is the mean function and $K(\mathbf{x}, \mathbf{x}')$ is a covariance kernel function for two sample points \mathbf{x} and \mathbf{x}' . A common kernel function is the Matérn kernel, defined as

$$K_M(\mathbf{x}, \mathbf{x}') = \frac{1}{\Gamma(\nu)2^{\nu-1}} \left(\frac{\sqrt{2\nu}}{l}d(\mathbf{x}, \mathbf{x}')\right)^\nu K_\nu\left(\frac{\sqrt{2\nu}}{l}d(\mathbf{x}, \mathbf{x}')\right) \quad (12)$$

where ν is the smoothness hyperparameter, Γ is the gamma function, l is the length scale, d is the Euclidean distance function, and K_ν is a modified Bessel function of the second kind. The Matérn kernel is appropriate for an objective function that changes significantly with small variations in the input variables. A small value of ν prevents over-smoothing of the objective function.

During each BO iteration, a new sample point is selected by maximizing an acquisition function. The acquisition function quantifies how promising a sample point is in finding the optimal solution. One example of an acquisition function is the upper confidence bound (UCB) function. For minimization, it is defined as

$$A_{UCB}(\mathbf{x}) = \alpha\sigma(\mathbf{x}) - \mu(\mathbf{x}) \quad (13)$$

where $\alpha > 0$ is a tradeoff parameter, $\sigma(\mathbf{x})$ is the standard deviation of the objective value, and $\mu(\mathbf{x})$ is the average objective value at \mathbf{x} . The value of α determines whether exploration or exploitation is favored. For a small value of α , the search process favors sample points with small objective values. For a large value of α , the search process favors sample points with large levels of uncertainty. After the next sample point is determined, the objective value is calculated, and the surrogate is updated with the new sample point. The optimization process continues until convergence criteria are met.

The kernel function affects the accuracy and precision of the GPR in estimating possible objective functions. For the TM-QABOA, the objective value is non-deterministic since a basis state is measured at random. The kernel function must incorporate the uncertainty associated with the basis state measurements to improve the precision of the objective value estimation. The novel QM kernel function which incorporates the uncertainty of the basis state measurements is presented in the following sub-section.

3.3. Quantum Matérn Kernel Function

The proposed QM kernel function is defined as

$$K_{QM} = K_M + K_Q \quad (14)$$

where K_M is the Matérn kernel defined in Eq. (12), and

$$K_Q(\mathbf{x}, \mathbf{x}') = \begin{cases} \omega(\kappa + \varepsilon)^{-2} & (\mathbf{x} = \mathbf{x}') \\ 0 & (\mathbf{x} \neq \mathbf{x}') \end{cases} \quad (15)$$

is a new quantum kernel as a function of the Pearson kurtosis κ of the estimated basis state distribution, where $\omega > 0$ is a scaling hyperparameter, and ε is a small positive value to prevent the division by zero.

Suppose z is an integer-valued random variable such that $z = 0, 1, \dots, 2^n - 1$ corresponds to the n -qubit basis states $|00\dots00\rangle, |00\dots01\rangle, \dots, |11\dots11\rangle$, respectively. The Pearson kurtosis for z is calculated as

$$\kappa = \frac{\xi}{\sigma^4} \quad (16)$$

where $\xi = \int (z - \mu)^4 p(z) dz$ is the fourth central moment, μ is the mean, and σ is the standard deviation. The value of κ indicates how sharp the peak of the distribution is. A very large value of κ for the basis state distribution means that a few amplitudes are significantly larger than the rest. In this case, the uncertainty associated with the quantum circuit measurement is small. As κ increases, the uncertainty of the basis state measurement decreases quadratically.

In the QM kernel function, the key aspect for improving the searching efficiency is the addition of K_Q . Since the basis state measurements are stochastic in nature, the optimization process is susceptible to the variation in the objective evaluations. For this reason, K_Q depends on the kurtosis which represents the consistency of basis state measurements. Adding K_Q to K_M allows the objective values at sample points to vary, which increases the number of possible objective functions described by the distribution of the probabilistic GPR. In turn, there is a higher chance that the objective values at the new sample points become closer to the optimal solution. Furthermore, K_Q depends on the scaling hyperparameter ω , which captures the extent of the variation in objective values at the known sample points. As the search process proceeds, ω is tuned with the L-BFGS-B algorithm so that the optimal solution can be obtained in fewer iterations. Therefore, the convergence towards the optimal solutions can be accelerated. The proposed QM kernel is used in the surrogate model of the new uTM-QABOA.

3.4. Proposed uTM-QABOA Procedure

In the proposed uTM-QABOA, Monte Carlo sampling is performed on the same quantum circuit of TM-QABOA in FIGURE 1 to estimate the basis state distribution so that the kurtosis can be calculated.

TABLE 1. uTM-QABOA procedure.

INPUT: $Num_init_samples, Num_BO_iter, Num_MC$	
OUTPUT: $\mathbf{x}^*, f(\mathbf{x}^*)$	
(1)	$i = 0, D = \emptyset, K = \emptyset,$
(2)	WHILE $i < Num_init_samples$:
(3)	Sample a point $\mathbf{x} = (\gamma_1, \beta_1, \theta_1, \dots, \gamma_p, \beta_p, \theta_p, \mathbf{x}_c)$ from search space
(4)	$j = 0, B = \emptyset$
(5)	WHILE $j < Num_MC$:
(6)	Run quantum circuit in Eq. (2) with \mathbf{x}
(7)	Measure $ \psi_f\rangle$ from the quantum circuit and insert to B
(8)	$j = j + 1$
(9)	END WHILE
(10)	Compute κ from B and insert to K
(11)	Compute $f = f(\mathbf{x}_c, \psi_m\rangle)$
(12)	Insert $\{\mathbf{x}, f\}$ to D
(13)	$i = i + 1$
(14)	END WHILE
(15)	Train GPR on D
(16)	$i = 0$
(17)	WHILE $i < Num_BO_iter$ and convergence criteria are not met:
(18)	Find $\mathbf{x}^\dagger = \underset{\mathbf{x}}{\operatorname{argmax}} A(\mathbf{x})$
(19)	$j = 0, B = \emptyset$
(20)	WHILE $j < Num_MC$:
(21)	Run quantum circuit in Eq. (2) with \mathbf{x}^\dagger
(22)	Measure $ \psi_f\rangle$ from the quantum circuit and insert to B
(23)	$j = j + 1$
(24)	END WHILE
(25)	Compute κ from B and insert to K
(26)	Compute $f^\dagger = f(\mathbf{x}_c^\dagger, \psi_m\rangle)$
(27)	IF $f^\dagger < f^*$:
(28)	$\mathbf{x}^* = \mathbf{x}^\dagger, f^* = f^\dagger$
(29)	END IF
(30)	Insert $\{\mathbf{x}^\dagger, f^\dagger\}$ to D
(31)	Update GPR on D
(32)	$i = i + 1$
(32)	END WHILE

TABLE 1 shows the uTM-QABOA procedure. First, initial samples of the rotation angles $\gamma_i, \beta_i, \theta_i$ ($i = 1, \dots, p$) and continuous variables \mathbf{x}_c are randomly acquired from the search space. For each initial sample, the quantum circuit defined in Eq. (2) is performed for multiple runs. During each run, a basis state $|\psi_f\rangle$ is measured and the result is stored in the set B . The kurtosis κ of the basis state distribution is computed after those runs and stored in the set K . The objective value f of each sample point \mathbf{x} is computed with the most frequently measured basis state $|\psi_m\rangle$. The sample $\{\mathbf{x}, f\}$ is added to the dataset of known sample points D . The GPR with the QM kernel is then trained on the initial sample points. The GPR hyperparameters are tuned during the training process. After the initial GPR model is constructed, the next sample point \mathbf{x}^\dagger is determined by maximizing the acquisition function $A(\mathbf{x})$ in each iteration. The quantum circuit is performed for several runs to approximate the basis state distribution, from which κ is computed. The new objective value f^\dagger is also computed with $|\psi_m\rangle$. The current best sample \mathbf{x}^* and its objective value f^* are then updated if the new objective value is better than the current best one. The new sample $\{\mathbf{x}^\dagger, f^\dagger\}$ is added to D , and the GPR is updated. The optimization process continues until convergence criteria are met.

Multiple runs of the quantum circuit are needed to compute the kurtosis of the basis state distribution. Given the probabilistic nature of the basis state measurements, QAOA's are usually run multiple times to receive reliable results. Therefore, uTM-QABOA does not increase the computational cost significantly.

4. Optimization Examples

In this section, TM-QABOA and uTM-QABOA are demonstrated with nine optimization problems. The first problem, discussed in Section 4.1, is unweighted MaxCut with a complete graph of six vertices. The next three problems, discussed in Section 4.2, are weighted MaxCut problems with complete graphs of five vertices. The fifth problem, discussed in Section 4.3, is lattice protein folding. The sixth problem, discussed in Section 4.4, is potential energy minimization of the ionic helium hydride (HeH^+) molecule. The seventh problem, discussed in Section 4.5, is the design of a welded beam. The eighth problem, discussed in Section 4.6, is the design of a speed reducer. The ninth problem, discussed in Section 4.7, is the design of a cylindrical pressure vessel. The first five examples involve discrete search spaces, whereas the last four examples involve mixed-integer search spaces.

For all nine examples, TM-QABOA and uTM-QABOA are compared with three single-mixer QABOA's, which include X-QABOA, XY-QABOA, and GM-QABOA, where the same BO framework is applied to optimize rotation angles and continuous variables. X-QABOA consists of Pauli-X mixers, XY-QABOA consists of XY-graph mixers, and GM-QABOA consists of generalized Grover mixers.

4.1. MaxCut Problem with 6-Complete Graph

Let $G(V, E)$ be a graph where V and E are the sets of vertices and edges of G , respectively. Suppose V is partitioned into two non-overlapping subsets V_0 and V_1 . The objective of the MaxCut problem is to maximize the number of edges in E connecting vertices between V_0 and V_1 . The objective function is defined as

$$f(\mathbf{q}) = \sum_{\{i,j\} \in E} (q_i + q_j - 2q_i q_j) \quad (17)$$

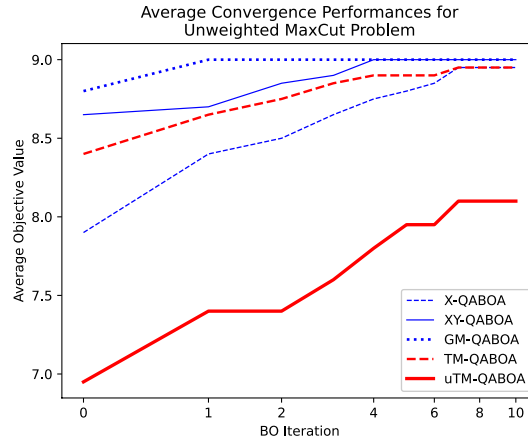
where q_i ($i = 1, \dots, n$) indicates whether the vertex i belongs to V_0 (if $q_i = 0$) or V_1 (if $q_i = 1$). n is the total number of vertices. $\mathbf{q} = (q_1, q_2, \dots, q_n)$ is a combinatorial choice of vertices and (i, j) denotes the edge between vertices i and j . Since there are n binary variables, n qubits are needed to solve the problem.

In this example, the MaxCut problem is solved with a complete graph of six vertices. Each of the five algorithms is performed twenty times to determine the average convergence performances. All algorithms consist of six rotation angles to keep the dimension of the search space the same. For X-QABOA, XY-QABOA, and GM-QABOA, two rotation angles γ_i and β_i ($i = 1, 2, 3$) are repeated three times. For TM-QABOA and uTM-QABOA, three rotation angles γ_i , β_i , and θ_i ($i = 1, 2$) are repeated twice. All rotation angles range from 0 to 2π .

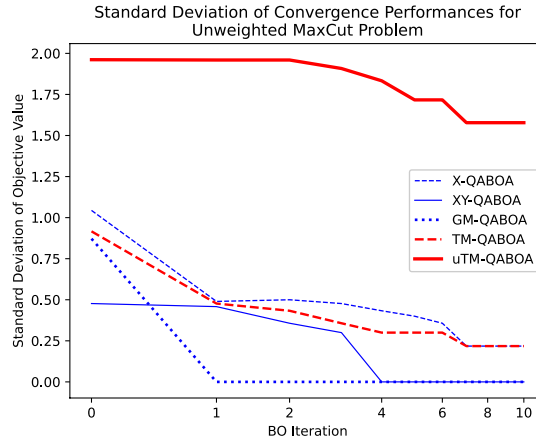
The initial dataset to construct the initial GPR model consists of three sample points. Each sample point corresponds to six values of the rotation angles. The same initial dataset is used to initialize the GPR models in all five algorithms for the purpose of comparison. The initial values of γ_1 , β_1 , γ_2 , and β_2 are the same for all algorithms. The initial values of θ_1 and θ_2 are the same for TM-QABOA and uTM-QABOA. For X-QABOA, XY-QABOA, and GM-QABOA, γ_3 and β_3 are initialized as zeroes to maintain the same circuit depth. Each run occurs for 10 BO iterations since the global optimum can be quickly obtained from 64 possible solutions. The GPR is defined with the Matérn kernel for all algorithms except uTM-QABOA. The value of ν is set to 0.5 for both Matérn and QM kernels to model large objective value changes with small rotation angle changes. The acquisition function for all algorithms is UCB, which allows for the ease of controlling the balance between exploration and exploitation by setting the α value in Eq. (13). Here, α is set to 1. The acquisition function is maximized by simulated annealing for 50 iterations.

FIGURE 2(a) and (b) show the averages and standard deviations of the best observed objective values, respectively. In FIGURE 2(a), GM-QABOA is the fastest to converge towards the global maximum value of 9. By the first iteration, all twenty runs of GM-QABOA result in the global optimal solution. Meanwhile, uTM-QABOA converges the slowest towards the global optimum. However, at the early stage of optimization, it is possible for uTM-QABOA to converge towards the global optimum. For instance, after the first iteration, uTM-QABOA

results in an average best value of 7.4 with a standard deviation of 1.96. The global optimum is within one standard deviation of the average value. The performance of TM-QABOA is similar to those of other algorithms.



(a)



(b)

FIGURE 2. (a) Averages and (b) standard deviations for the best observed objective values for the MaxCut problem.

4.2. Weighted MaxCut Problem with 5-Complete Graphs

A generalized version of the MaxCut problem is the weighted MaxCut problem, where each edge (i, j) has a weight value W_{ij} . The objective of the weighted MaxCut problem is to maximize the total sum of weights associated with edges connecting vertices between V_0 and V_1 . The objective function is defined as

$$f(\mathbf{q}) = \sum_{\{i,j\} \in E} W_{ij}(q_i + q_j - 2q_i q_j). \quad (18)$$

This function is similar to Eq. (17), except that each term in the sum is multiplied by W_{ij} .

In this example, the weighted MaxCut problem is solved on three instances of a complete graph with 5 vertices. The graph is illustrated in FIGURE 3. Three sets of weight values are randomly generated as listed in TABLE 2. The global maximum values are 32.3 for Graph 1, 36.4 for Graph 2, and 38.5 for Graph 3. Since the problem involves five binary variables q_i ($i = 1, 2, 3, 4, 5$), five qubits are needed to solve the problem.

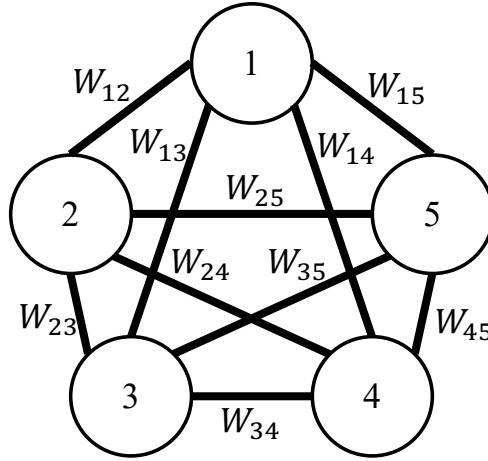
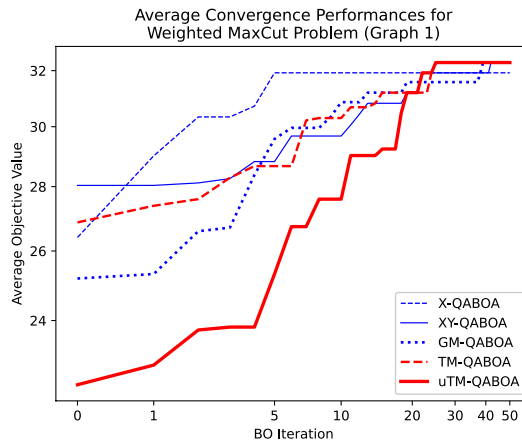


FIGURE 3. 5-complete graph with edge weights.

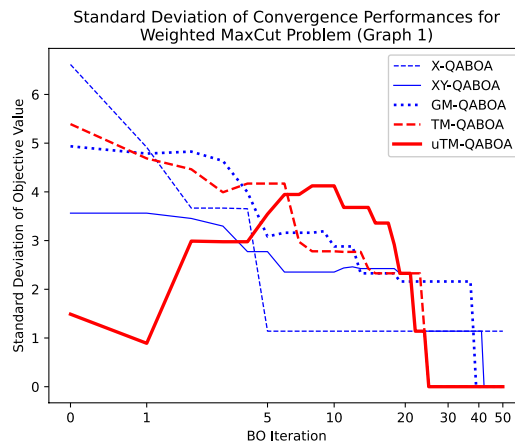
TABLE 2. Randomly generated edge weight values for three 5-complete graphs.

(i, j)	W_{ij}		
	Graph 1	Graph 2	Graph 3
(1, 2)	6.5	1.9	9.2
(1, 3)	2.7	7.9	1.4
(1, 4)	1.6	7.9	2.0
(1, 5)	5.0	1.4	6.0
(2, 3)	5.7	0.4	1.7
(2, 4)	3.1	0.4	1.6
(2, 5)	0.9	0.1	9.9
(3, 4)	1.0	3.1	10.0
(3, 5)	8.7	9.3	5.8
(4, 5)	3.3	9.3	5.7

For every graph instance, the five algorithms are repeated ten times. Each algorithm consists of six rotation angles to maintain a constant search space dimension, similarly to the previous example. For all runs of each algorithm, the same initial dataset of three sample points is used, where each sample point consists of six rotation angles. Each run is performed for 50 BO iterations since the algorithms can find the global optimum quickly from 32 possible solutions. The GPR is defined with the QM kernel for uTM-QABOA or the Matérn kernel for all other algorithms. ν is set to 0.5 for both kernels. All algorithms are performed with the UCB acquisition function with α set to 1. 20,000 simulated annealing steps are performed to maximize the UCB function.



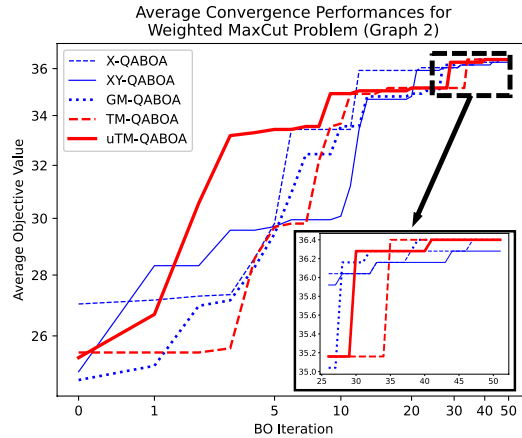
(a)



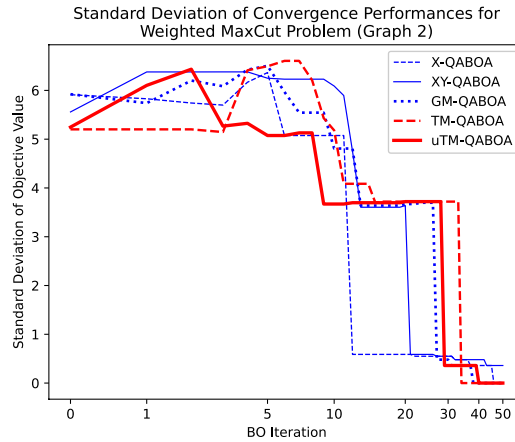
(b)

FIGURE 4. (a) Averages and (b) standard deviations for the best observed objective values for the weighted MaxCut problem with Graph 1.

FIGURE 4, 5, and 6 show the averages and standard deviations of the best observed objective values for Graphs 1, 2, and 3, respectively. For Graphs 1 and 2, TM-QABOA more quickly converges to the global optimum than the single-mixer methods as shown in FIGURE 4(a) and 5(a). For those two graphs, TM-QABOA exhibits lower standard deviation than the single-mixer algorithms as shown in FIGURE 4(b) and 5(b), meaning that the convergence performance of TM-QABOA is more consistent.



(a)

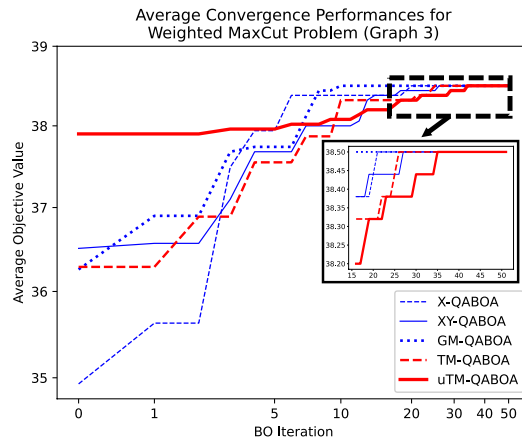


(b)

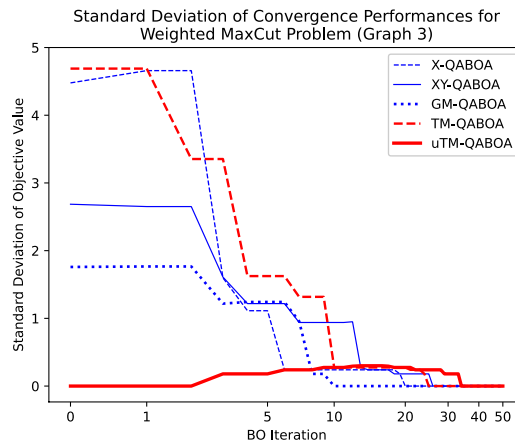
FIGURE 5. (a) Averages and (b) standard deviations for the best observed objective values for the weighted MaxCut problem with Graph 2.

As shown in FIGURE 4(a), uTM-QABOA achieves a higher objective value than TM-QABOA before converging to the global maximum. Therefore, uTM-

QABOA results in the highest searching efficiency for Graph 1. In FIGURE 4(b), uTM-QABOA has the most consistent convergence performance since it has a lower standard deviation than TM-QABOA before converging to the global optimum. For Graph 2, uTM-QABOA is outperformed by GM-QABOA and TM-QABOA. However, it is possible for uTM-QABOA to converge to the global optimum in fewer iterations. At iteration 34, during which TM-QABOA converges to the global optimum, uTM-QABOA results in an average value of 36.28 with a standard deviation of 0.36 in FIGURE 5(a) and (b). In this case, the global optimum is located within one standard deviation of the mean value.



(a)



(b)

FIGURE 6. (a) Averages and (b) standard deviations for the best observed objective values for the weighted MaxCut problem with Graph 3.

For Graph 3, TM-QABOA is outperformed by X-QABOA and GM-QABOA, where GM-QABOA converges most quickly to the optimal solution at iteration 10. However, at the same iteration, TM-QABOA results in an average value of 38.32 with a standard deviation of 0.27 in FIGURE 6(a) and (b). Since the global optimum is located within a standard deviation of the mean value, it is possible for TM-QABOA to converge to the global optimum in fewer iterations. The performance of uTM-QABOA is similar to that of TM-QABOA.

It is also observed from all three graphs that GM-QABOA converges to the global optimum more quickly than both X-QABOA and XY-QABOA. Therefore, it is suggested that exploitation through amplitude amplification is important to improve searching efficiency.

4.3. Lattice Protein Folding

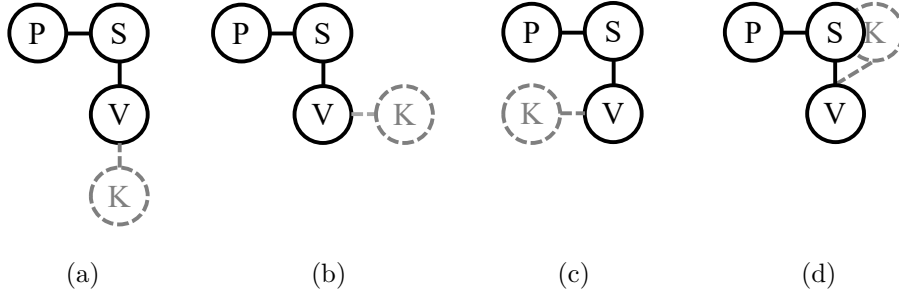


FIGURE 7. The PSVK sub-sequence where (a) K is south of V, (b) K is east of V, (c) K is west of V, and (d) K is north of V.

Protein folding is the process where a chain of amino acids is folded into a three-dimensional protein structure. In the two-dimensional lattice protein folding problem, there are four choices for the directions of the amino acid bonds: up, down, left, and right. Suppose a chain consists of six amino acids in the following order [35]: proline (P), serine (S), valine (V), lysine (K), methionine (M), and alanine (A). The directionality of the PSVKMA chain is then represented by the binary sequence $q_a q_b q_c q_d q_e q_f q_g q_h q_i q_j$. The pair $q_a q_b$ represents the direction from P to S, $q_c q_d$ represents the direction from S to V, $q_e q_f$ represents the direction from V to K, $q_g q_h$ represents the direction from K to M, and $q_i q_j$ represents the direction from M to A. Each two-qubit pair has four choices which include 00 (south), 01 (east), 10 (west), and 11 (north). For instance, suppose that S is east of P and V is south of S. Then the binary representation of the PSVKMA sequence is $0100q_1q_2q_3q_4q_5q_6$, where q_1 to q_6 need to be determined in the subsequent folding process. This example is to decide the six remaining folding parameters so as to minimize the energy of the protein. FIGURE 7 shows the four possible configurations of the PSVK sub-sequence. The configuration in FIGURE 7(a) is encoded by $010000q_3q_4q_5q_6$. The configuration in FIGURE

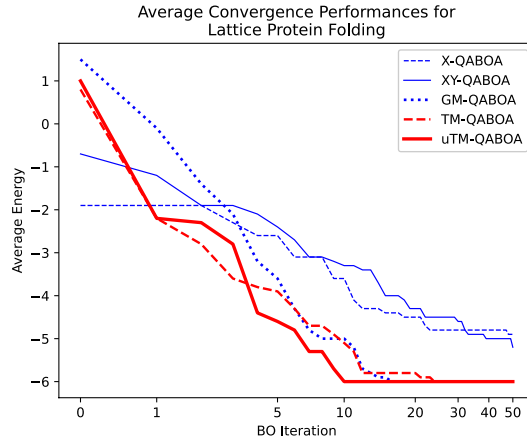
7(b) is encoded by $010001q_3q_4q_5q_6$. The configuration in FIGURE 7(c) is encoded by $010010q_3q_4q_5q_6$. The configuration in FIGURE 7(d) is encoded by $010011q_3q_4q_5q_6$.

The objective function is

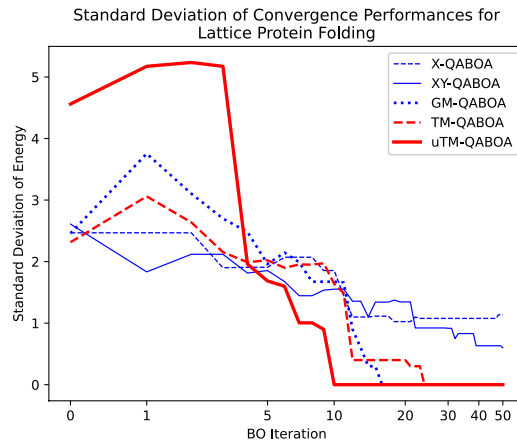
$$\begin{aligned}
f(q_1, q_2, q_3, q_4, q_5, q_6) = & -q_1 + 15q_1q_2 + 4q_2q_3 - 6q_1q_2q_3 + 4q_1q_4 \\
& -15q_1q_2q_4 + 15q_3q_4 - 6q_1q_3q_4 - 15q_2q_3q_4 + 28q_1q_2q_3q_4 - 4q_2q_5 \\
& + 2q_1q_2q_5 + 2q_2q_3q_5 + 4q_1q_2q_3q_5 + 7q_4q_5 + 7q_5q_6 + 2q_1q_4q_5 \\
& + 4q_2q_4q_5 + 9q_1q_2q_4q_5 - 20q_3q_4q_5 + 4q_1q_3q_4q_5 + 9q_2q_3q_4q_5 \\
& - 37q_1q_2q_3q_4q_5 - 4q_1q_6 + 4q_1q_2q_6 + 7q_3q_6 + 2q_1q_3q_6 + 4q_2q_3q_6 \\
& + 9q_1q_2q_3q_6 + 4q_1q_4q_6 - 18q_3q_4q_6 + 9q_1q_3q_4q_6 - 33q_1q_2q_3q_4q_6 \\
& + 2q_1q_5q_6 + 4q_2q_5q_6 - 20q_3q_5q_6 + 9q_1q_2q_5q_6 + 4q_1q_3q_5q_6 \\
& + 9q_2q_3q_5q_6 - 37q_1q_2q_3q_5q_6 - 18q_4q_5q_6 + 9q_1q_4q_5q_6 - 33q_1q_2q_4q_5q_6 \\
& + 53q_3q_4q_5q_6 - 37q_1q_3q_4q_5q_6 - 33q_2q_3q_4q_5q_6 + 99q_1q_2q_3q_4q_5q_6.
\end{aligned} \tag{19}$$

The BO search space consists of six rotation angles for the quantum circuit. Each of the q_i 's in Eq. (19) is implemented with a Pauli-Z gate as in Eq. (4). Similar to the previous example, the GPR models for all five algorithms are initialized with the same initial dataset of three sample points, where each sample point corresponds to six values of rotation angles. Each algorithm is repeated for ten runs, where each run is performed for 50 BO iterations since the global optimum is easily obtained from 64 possible solutions. The value of ν is set to 0.5 for both the Matérn kernel in Eq. (12) and QM kernel in Eq. (14). The acquisition function is the UCB function in Eq. (13), where the value of α is set to 1. 20,000 simulated annealing steps are performed to find the next sample point.

FIGURE 8(a) and (b) show the averages and standard deviations for the best observed objective values, respectively. In FIGURE 8(a), GM-QABOA, TM-QABOA, and uTM-QABOA converge to the global minimum value of -6 in less than 50 iterations. Among all five algorithms, uTM-QABOA converges to the global optimum in the fewest iterations. It is also observed that GM-QABOA converges to the global optimum in fewer iterations than TM-QABOA. This suggests that the exploitation capability is helpful in improving the searching efficiency. In FIGURE 8(b), uTM-QABOA has the lowest standard deviation after about 5 iterations. This means that uTM-QABOA exhibits the most consistent convergence performance towards the global optimum out of all five algorithms.



(a)



(b)

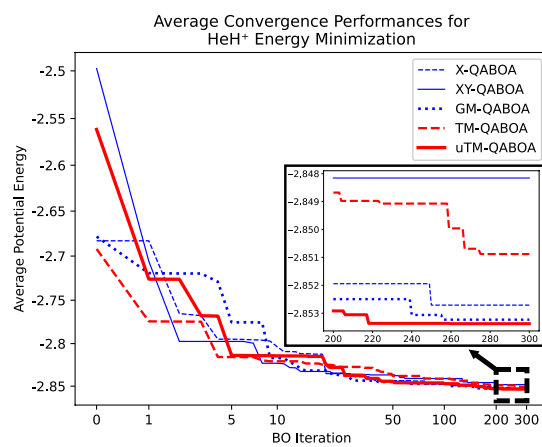
FIGURE 8. (a) Averages and (b) standard deviations for the best observed energy values for the lattice protein folding problem.

4.4. Potential Energy Minimization of the Ionic Helium Hydride Molecule

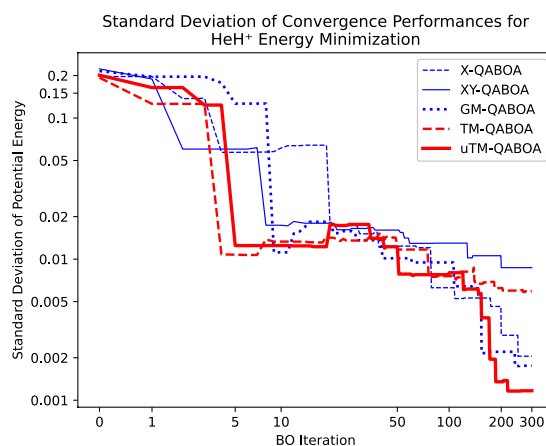
The objective of this problem is to minimize the potential energy of the HeH^+ molecule. Two types of variables are considered. The first type is the bond length L between the helium and hydrogen atoms, which continuously ranges from 0.1 to 3 Å. The second type is the orbital configuration, which is represented by binary variables.

The orbital configuration of HeH^+ can be fully represented with four qubits, each of which corresponds to a spin orbital. For a molecular Hamiltonian, the

number of qubits can be reduced with the qubit tapering technique [36]. In qubit tapering, those Pauli operators which commute with the molecular Hamiltonian are determined. These Pauli operators encode the symmetries of the Hamiltonian. A new Hamiltonian with a smaller size is computed from these Pauli operators and used in computing the energy instead of the original Hamiltonian. For HeH^+ , qubit tapering reduces the number of qubits from four to two. Therefore, two binary variables represent the orbital configuration of the molecule.



(a)



(b)

FIGURE 9. (a) Averages and (b) standard deviations for the best observed potential energy values for the HeH^+ energy minimization problem.

Each of the five algorithms is repeated for ten runs, where each run is performed for 300 BO iterations. Compared to the previous three examples, the number of

BO iterations is much larger. It is expected that finding the global optimum for continuous variables is more difficult. The initial dataset for all runs consists of the same five sample points randomly sampled from the search space. Each sample point corresponds to the six values of rotation angles and one value of L . The phase-separating Hamiltonian is the qubit-tapered molecular Hamiltonian computed with the PennyLane Python library. The quantum circuit is performed on two qubits which represent the orbital configuration of HeH^+ . The value of ν is 0.5 for both the Matérn and QM kernels. The acquisition function is the UCB function with α set to 1, where this function is maximized with 20,000 simulated annealing steps.

FIGURE 9(a) and (b) show the averages and standard deviations for the best observed objective values, respectively. The closer view in FIGURE 9(a) shows the convergence during the last 100 iterations. Overall, uTM-QABOA exhibits the best optimization performance. In FIGURE 9(a), uTM-QABOA results in the lowest average objective value after 300 iterations. This is a noticeable improvement over TM-QABOA, which converges to a higher average objective value than X-QABOA and GM-QABOA. GM-QABOA exhibits the second highest searching efficiency, which suggests the importance of exploitation in improving the searching efficiency. In FIGURE 9(b), uTM-QABOA has the lowest standard deviation after about 200 iterations.

4.5. Welded Beam Design

FIGURE 10 illustrates a welded beam [37] subjected to a downward point load of $F = 6,000$ lb at the free end. The beam length is known to be $L = 14$ in. The continuous design variables \mathbf{x}_c include the weld thickness h , the welded joint length l , the beam width t , and the beam thickness b . Two discrete design variables include the weld type w and the bulk material type m .

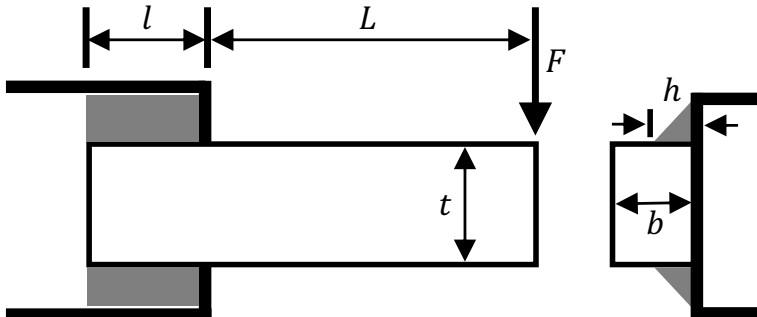


FIGURE 10. Welded beam design problem.

The objective of the problem is to minimize the cost of the welded beam, defined as

$$f(w, m, h, l, t, b) = (1 + C_1(m))(wt + l)h^2 + C_2(m)tb(L + l) \quad (20)$$

where $C_1(m)$ and $C_2(m)$ are the costs per volume of the welded material and bar stock, respectively. C_1 and C_2 depend on material type m . The design variables are subjected to a buckling load constraint defined as

$$b - h \geq 0. \quad (21)$$

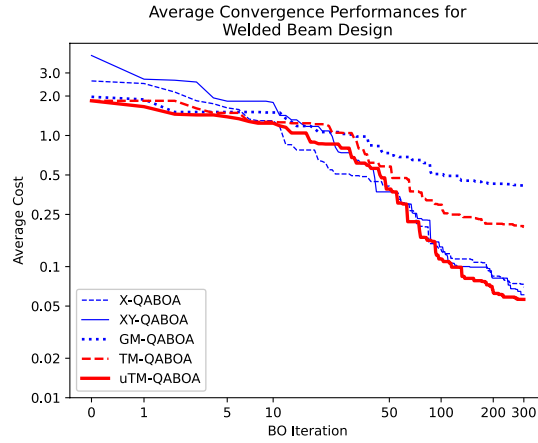
It is noted that this problem is a simplified version of the original welded beam design problem [38], where additional constraints are imposed.

For the continuous variables, $0.0625 \text{ in} \leq h \leq 2 \text{ in}$, $0.1 \text{ in} \leq l \leq 10 \text{ in}$, $2 \text{ in} \leq t \leq 20 \text{ in}$, and $0.0625 \text{ in} \leq b \leq 2 \text{ in}$. The discrete variable w is set to 0 or 1 for two-sided and four-sided welding, respectively. The discrete variable m is set to 1, 2, 3, or 4 which corresponds to steel, cast iron, aluminum, and brass, respectively. When $m = 1$, $C_1 = \$0.1047 \text{ in}^{-3}$ and $C_2 = \$0.0481 \text{ in}^{-3}$. When $m = 2$, $C_1 = \$0.0489 \text{ in}^{-3}$ and $C_2 = \$0.0224 \text{ in}^{-3}$. When $m = 3$, $C_1 = \$0.5235 \text{ in}^{-3}$ and $C_2 = \$0.2405 \text{ in}^{-3}$. When $m = 4$, $C_1 = \$0.5584 \text{ in}^{-3}$ and $C_2 = \$0.2566 \text{ in}^{-3}$.

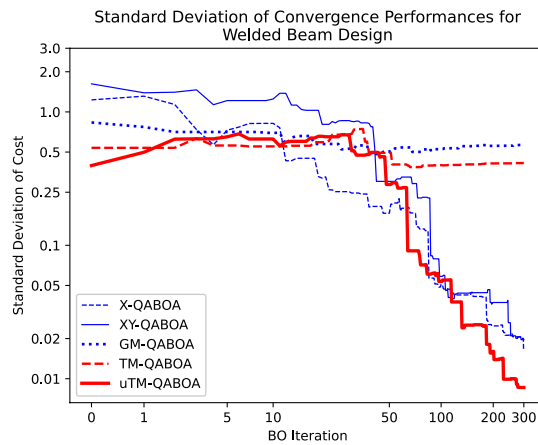
Since there are two choices for w and four choices for m , the optimization problem is solved with a three-qubit system. The objective function in Eq. (20) can be reformulated as the function in Eq. (25) in Appendix, where q_1 is a binary variable which corresponds to values of w , and q_2 and q_3 are binary variables which correspond to values of m .

Each of the five algorithms is repeated for ten runs, where each run is performed for 300 BO iterations. The initial dataset is constructed with ten sample points randomly acquired from the search space. Each sample point corresponds to the six values of rotation angles, and four values for the continuous variables. The value of ν is set to 0.5 for both the Matérn and QM kernels. The UCB acquisition function, with α set to 1, is maximized with 20,000 simulated annealing steps. If the buckling load constraint is violated at a sample point, the UCB function value is set to -100,000 to prevent the sample point from being selected.

Out of all the tested algorithms, uTM-QABOA exhibits the best optimization performance. As shown in FIGURE 11(a), uTM-QABOA results in the lowest average objective value after 300 iterations. It also has the lowest standard deviation after about 100 iterations, as shown in FIGURE 11(b).



(a)



(b)

FIGURE 11. (a) Averages and (b) standard deviations for the best observed cost values for the welded beam design problem.

Meanwhile, after 300 iterations, TM-QABOA results in a higher average objective value than X-QABOA, XY-QABOA, and uTM-QABOA. Nevertheless, the standard deviation of TM-QABOA is also higher than those of the other three algorithms. This indicates that the performance of TM-QABOA is not consistent, although it may sometimes result in better objective values. The performance of GM-QABOA is similar to that of TM-QABOA, which again shows the importance of exploitation consideration.

4.6. Speed Reducer Design

The objective of this problem is to minimize the weight of a speed reducer, defined as [37]

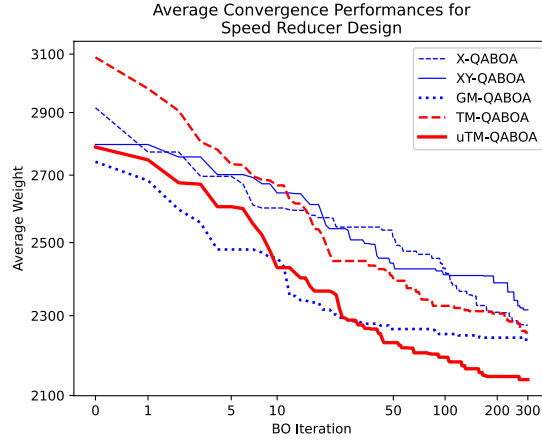
$$\begin{aligned}
 f(x_1, x_2, x_3, x_4, x_5, x_6, x_7) = & 0.7854x_1x_2^2(3.3333x_3^2 + 14.9334x_3 \\
 & - 43.0934) - 1.508x_1(x_6^2 + x_7^2) + 7.4777(x_6^3 + x_7^3) \\
 & + 0.7854(x_4x_6^2 + x_5x_7^2),
 \end{aligned} \tag{22}$$

where $x_1, x_2, x_3, x_4, x_5, x_6$, and x_7 are the face weight, module of teeth, number of pinion teeth, length of the first shaft between bearings, length of the second shaft between bearings, first shaft diameter, and second shaft diameter, respectively. x_3 is an integer-valued variable with 16 choices ranging from 15 to 30. The continuous variables \mathbf{x}_c include x_1, x_2, x_4, x_5, x_6 , and x_7 . The ranges for the continuous variables are $2.6 \leq x_1 \leq 3.6$, $0.7 \leq x_2 \leq 0.8$, $7.3 \leq x_4 \leq 8.3$, $7.8 \leq x_5 \leq 8.3$, $2.9 \leq x_6 \leq 3.9$, and $5 \leq x_7 \leq 5.5$. In this work, the constraints of the original speed reducer design problem [39] are ignored.

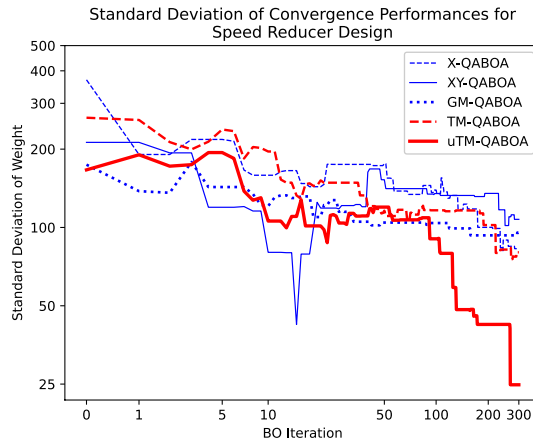
The problem is solved with four qubits since there are 16 choices for x_3 . The objective function in Eq. (22) can be reformulated as the function in Eq. (26) in Appendix, where q_1, q_2, q_3 , and q_4 are binary variables which correspond to values of x_3 .

Each of the five algorithms is repeated for ten runs, where each run is performed for 300 BO iterations. The initial dataset is constructed with 10 sample points randomly acquired from the search space. Each sample point corresponds to the six values of rotation angles, and six values of the continuous variables. The value of ν for the Matérn and QM kernels is set to 0.5. The UCB acquisition function, with α set to 1, is maximized with 20,000 simulated annealing steps.

As shown in FIGURE 12(a), uTM-QABOA converges to the lowest average objective value after 300 iterations. In FIGURE 12(b), uTM-QABOA results in the lowest standard deviation after about 100 iterations. There are noticeable improvements in both average and standard deviation over TM-QABOA. It is also observed that GM-QABOA results in the second lowest average objective value after 300 iterations. This also suggests that exploitation is important in finding the optimal solution efficiently.



(a)



(b)

FIGURE 12. (a) Averages and (b) standard deviations for the best observed weight values for the speed reducer design problem.

4.7. Pressure Vessel Design

The objective of this problem is to minimize the cost of a cylindrical pressure vessel, defined as [37]

$$f(x_1, x_2, x_3, x_4) = 0.6224x_1x_3x_4 + 1.7781x_2x_3^2 + 3.1661x_1^2x_4 + 19.84x_1^2x_3, \quad (23)$$

where x_1 is the hemisphere thickness, x_2 is the cylindrical shell thickness, x_3 is the hemisphere inner radius, and x_4 is the cylinder length. The design variables are subjected to a volume constraint defined as

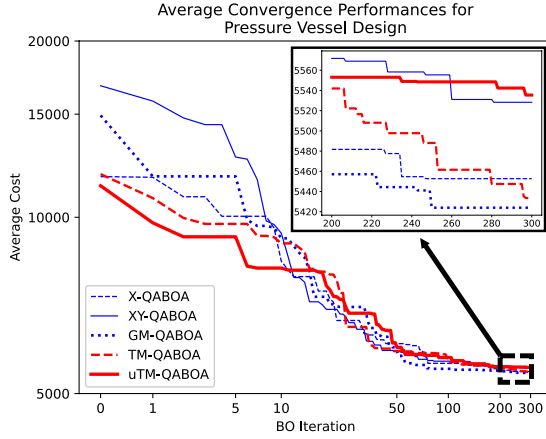
$$-\pi x_3^2 x_4^2 - \frac{4}{3} x_3^3 + 1296000 \leq 0. \quad (24)$$

In this problem, x_1 and x_2 are integer-valued variables each ranging from 3 to 6. The continuous variables \mathbf{x}_c include x_3 and x_4 which each range from 10 to 150. The variable values are set so that all constraints of the original pressure vessel design problem [39] are satisfied. Since there are 16 possible combinations of x_1 and x_2 , four qubits are needed to solve the problem. The objective function defined in Eq. (23) can be reformulated as the function in Eq. (27) in Appendix, where q_1 and q_2 correspond to values of x_1 , and q_3 and q_4 correspond to values of x_2 .

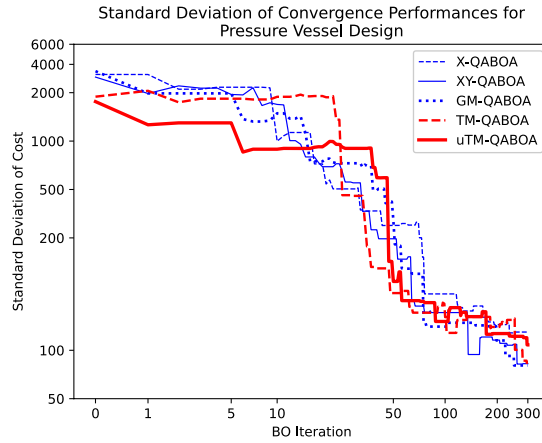
Each of the five algorithms is repeated for ten runs, where each run is performed for 300 BO iterations. The initial dataset is constructed with ten random sample points. Each sample point corresponds to the six values of rotation angles, and two values of continuous variables. The value of ν is set to 0.5 for both the Matérn and QM kernels. The UCB acquisition function, with α set to 1, is maximized with 20,000 simulated annealing steps. If the volume constraint is violated for a sample point, the UCB function value is set to $-10,000,000$ to prevent the sample point from being selected.

FIGURE 13(a) and (b) show the averages and standard deviations of the best observed objective values, respectively. The closer view in FIGURE 13(a) shows the convergence during the last 100 iterations. The averages from all five algorithms are very similar. uTM-QABOA has the highest value. Nevertheless, the difference between the objective values of uTM-QABOA and GM-QABOA is 111.5. The standard deviation of the best objective values of uTM-QABOA is 108.0. With the large standard deviation, uTM-QABOA may still obtain the lowest objective value.

In this example, GM-QABOA converges to the lowest objective value on average with the smallest standard deviation. It has the best performance out of the five algorithms. Similar to the previous five examples, amplitude amplification has shown the benefit of improving the searching efficiency, where solutions with better objective values are more favorably selected. The performance of TM-QABOA is similar to that of GM-QABOA. In this case, TM-QABOA converges to the second lowest objective value on average with a slightly higher standard deviation than GM-QABOA. The results of those two algorithms demonstrate the usefulness of exploitation and the importance of dynamic exploration-exploitation balance in achieving the optimal solution efficiently.



(a)



(b)

FIGURE 13. (a) Averages and (b) standard deviations for the best observed cost values for the pressure vessel design problem.

5. Concluding Remarks

In this paper, two versions of QAOA are proposed, where surrogate-based Bayesian optimization is used as the classical optimizer. They are named as TM-QABOA and uTM-QABOA. In TM-QABOA, the quantum circuit consists of two mixers to improve the exploration-exploitation balance. The Pauli-gate mixer is for exploration, while the generalized Grover mixer is for exploitation. In uTM-QABOA, a new QM kernel is proposed to consider the variation of objective values in the sampling process. The formulation based on the kurtosis

allows for the dynamic control of the variation based on the optimality of the objective values. As a result, this increases the chance of obtaining the optimum, thus improving the searching efficiency.

The proposed TM-QABOA and uTM-QABOA can be applied to solve mixed-integer problems. The rotation angles and continuous variables are optimized with Bayesian optimization, while the discrete variables are optimized through the quantum circuit. The new algorithms are tested with nine problems. They are compared with three single-mixer QABOA's, where the same Bayesian optimization framework is used as the classical optimizer. The results show that the proposed uTM-QABOA has the best performance in efficiency and consistency for five out of the nine tested problems. The results also show that GM-QABOA with the generalized Grover mixer performs the best among the three single-mixer algorithms, thereby demonstrating the benefit of exploitation in improving searching efficiency.

The purpose of TM-QABOA and uTM-QABOA is to improve the searching efficiency of QAOA's. QAOA's suffer from low searching efficiency when the circuit depth increases, since a large number of rotation angles need to be optimized. This is known as curse of dimensionality for optimization. The surrogate-based Bayesian optimization can improve the searching efficiency with the guidance of the GPR model. The results in this paper show the advantage of the proposed QABOA's. However, all nine test problems involve no more than seven variables and six qubits. For a small number of basis states, the performances of single mixers are reasonable. The Pauli-X mixer can drastically alter the amplitudes among a few basis states. As the number of basis states increases, the number of states with non-zero amplitudes increases and it is more difficult for the generalized Grover operator to increase the target basis amplitude to 1. For problems with larger numbers of qubits, the performance of the mixers could become worse. To fully understand the performance of QABOA's, larger problems with more qubits need to be studied in the future. In addition, TM-QABOA and uTM-QABOA are tested at low circuit depths in this paper. Sensitivity studies are also needed to evaluate the effect of circuit depths.

Similar to other quantum optimization algorithms, uTM-QABOA involves repeated sampling of the same quantum circuit to obtain a more reliable estimation of the optimum. The sampling is also used to approximate the basis state distributions in order to estimate the kurtosis in the QM kernel. To further improve the computational efficiency of uTM-QABOA, better sampling strategies are needed. For instance, variational inference can be applied where the basis state distributions are parametrized, and a smaller number of samples are needed to train and optimize those parameters.

Appendix

The modified objective function for the welded beam design problem is

$$\begin{aligned}
g(q_1, q_2, q_3, h, l, t, b) &= (1 - q_1)(1 - q_2)(1 - q_3)f(0, 1, h, l, t, b) \\
&+ (1 - q_1)(1 - q_2)q_3f(0, 2, h, l, t, b) + (1 - q_1)q_2(1 - q_3)f(0, 3, h, l, t, b) \\
&+ (1 - q_1)q_2q_3f(0, 4, h, l, t, b) + q_1(1 - q_2)(1 - q_3)f(1, 1, h, l, t, b) \\
&+ q_1(1 - q_2)q_3f(1, 2, h, l, t, b) + q_1q_2(1 - q_3)f(1, 3, h, l, t, b) \\
&+ q_1q_2q_3f(1, 4, h, l, t, b).
\end{aligned} \tag{25}$$

The modified objective function for the speed reducer design problem is

$$\begin{aligned}
&g(q_1, q_2, q_3, q_4, x_1, x_2, x_4, x_5, x_6, x_7) \\
&= (1 - q_1)(1 - q_2)(1 - q_3)(1 - q_4)f(x_1, x_2, 15, x_4, x_5, x_6, x_7) \\
&+ (1 - q_1)(1 - q_2)(1 - q_3)q_4f(x_1, x_2, 16, x_4, x_5, x_6, x_7) \\
&+ (1 - q_1)(1 - q_2)q_3(1 - q_4)f(x_1, x_2, 17, x_4, x_5, x_6, x_7) \\
&+ (1 - q_1)(1 - q_2)q_3q_4f(x_1, x_2, 18, x_4, x_5, x_6, x_7) \\
&+ (1 - q_1)q_2(1 - q_3)(1 - q_4)f(x_1, x_2, 19, x_4, x_5, x_6, x_7) \\
&+ (1 - q_1)q_2(1 - q_3)q_4f(x_1, x_2, 20, x_4, x_5, x_6, x_7) \\
&+ (1 - q_1)q_2q_3(1 - q_4)f(x_1, x_2, 21, x_4, x_5, x_6, x_7) \\
&+ (1 - q_1)q_2q_3q_4f(x_1, x_2, 22, x_4, x_5, x_6, x_7) \\
&+ q_1(1 - q_2)(1 - q_3)(1 - q_4)f(x_1, x_2, 23, x_4, x_5, x_6, x_7) \\
&+ q_1(1 - q_2)(1 - q_3)q_4f(x_1, x_2, 24, x_4, x_5, x_6, x_7) \\
&+ q_1(1 - q_2)q_3(1 - q_4)f(x_1, x_2, 25, x_4, x_5, x_6, x_7) \\
&+ q_1(1 - q_2)q_3q_4f(x_1, x_2, 26, x_4, x_5, x_6, x_7) \\
&+ q_1q_2(1 - q_3)(1 - q_4)f(x_1, x_2, 27, x_4, x_5, x_6, x_7) \\
&+ q_1q_2(1 - q_3)q_4f(x_1, x_2, 28, x_4, x_5, x_6, x_7) \\
&+ q_1q_2q_3(1 - q_4)f(x_1, x_2, 29, x_4, x_5, x_6, x_7) \\
&+ q_1q_2q_3q_4f(x_1, x_2, 30, x_4, x_5, x_6, x_7)
\end{aligned} \tag{26}$$

The modified objective function for the pressure vessel design problem is

$$\begin{aligned}
g(q_1, q_2, q_3, q_4, x_3, x_4) = & (1 - q_1)(1 - q_2)(1 - q_3)(1 - q_4)f(3, 3, x_3, x_4) \\
& + (1 - q_1)(1 - q_2)(1 - q_3)q_4f(3, 4, x_3, x_4) \\
& + (1 - q_1)(1 - q_2)q_3(1 - q_4)f(3, 5, x_3, x_4) \\
& + (1 - q_1)(1 - q_2)q_3q_4f(3, 6, x_3, x_4) \\
& + (1 - q_1)q_2(1 - q_3)(1 - q_4)f(4, 3, x_3, x_4) \\
& + (1 - q_1)q_2(1 - q_3)q_4f(4, 4, x_3, x_4) \\
& + (1 - q_1)q_2q_3(1 - q_4)f(4, 5, x_3, x_4) \\
& + (1 - q_1)q_2q_3q_4f(4, 6, x_3, x_4) \\
& + q_1(1 - q_2)(1 - q_3)(1 - q_4)f(5, 3, x_3, x_4) \\
& + q_1(1 - q_2)(1 - q_3)q_4f(5, 4, x_3, x_4) \\
& + q_1(1 - q_2)q_3(1 - q_4)f(5, 5, x_3, x_4) \\
& + q_1(1 - q_2)q_3q_4f(5, 6, x_3, x_4) + q_1q_2(1 - q_3)(1 - q_4)f(6, 3, x_3, x_4) \\
& + q_1q_2(1 - q_3)q_4f(6, 4, x_3, x_4) + q_1q_2q_3(1 - q_4)f(6, 5, x_3, x_4) \\
& + q_1q_2q_3q_4f(6, 6, x_3, x_4).
\end{aligned} \tag{27}$$

References

- [1] Y. Wang, J. E. Kim, and K. Suresh, "Opportunities and challenges of quantum computing for engineering optimization," *Journal of Computing and Information Science in Engineering*, vol. 23, no. 6, Aug. 2023, DOI. 10.1115/1.4062969
- [2] Y. Wang, "Global optimization with quantum walk enhanced Grover search," in 2014 ASME International Design Engineering Technical Conferences & The Computer and Information in Engineering Conference, Buffalo, NY, USA, 2014, DOI. 10.1115/DETC2014-34634.
- [3] Y. Wang, "Simulating stochastic diffusions by quantum walks," in 2013 ASME International Design Engineering Technical Conferences & The Computer and Information in Engineering Conference, Portland OR, USA, 2013, DOI. 10.1115/DETC2013-12739.
- [4] Y. Wang, "Accelerating stochastic dynamics simulation with continuous-time quantum walks," in 2016 ASME International Design Engineering Technical Conferences & The Computer and Information in Engineering Conference, Charlotte, NC, USA, 2016, DOI. 10.1115/DETC2016-59420.
- [5] E. Farhi, J. Goldstone, and S. Gutmann, "A quantum approximate optimization algorithm," 2014, *arXiv preprint arXiv:1411.4028*.
- [6] L. Zhou, S. T. Wang, S. Choi, H. Pichler, and M. D. Lukin, "Quantum approximate optimization algorithm: performance, mechanism, and im-

- plementation on near-term devices,” *Phys. Rev. X*, vol. 10, no. 2, pp. 021067, Jun. 2020, DOI. 10.1103/PhysRevX.10.021067.
- [7] Z. Wang, S. Hadfield, Z. Jiang, and E. G. Rieffel, “Quantum approximate optimization algorithm for MaxCut: a fermionic view,” *Phys. Rev. A*, vol. 97, no. 2, pp. 022304, Feb. 2018, DOI. 10.1103/PhysRevA.97.022304.
- [8] R. Shaydulin and S. M. Wild, “Exploiting symmetry reduces the cost of training QAOA,” *IEEE Transactions on Quantum Engineering*, vol. 2, pp. 1–9, Mar. 2021, DOI. 10.1109/TQE.2021.3066275.
- [9] R. Tate, M. Farhadi, C. Herold, G. Mohler, and S. Gupta, “Bridging classical and quantum with SDP initialized warm-starts for QAOA,” *ACM Transactions of Quantum Computing*, vol. 4, no. 2, pp. 1–39, Feb. 2023, DOI. 10.1145/3549554.
- [10] J. Cook, S. Eidenbenz, and A. Bärtschi, “The quantum alternating operator ansatz on maximum k-vertex cover,” in *2020 IEEE International Conference on Quantum Computing and Engineering (QCE)*, Denver, CO, USA, 2020, pp. 83–92. DOI. 10.1109/QCE49297.2020.00021.
- [11] C. Campbell and E. Dahl, “QAOA of the highest order,” in *2022 IEEE 19th International Conference on Software Architecture Companion (ICSA-C)*, Honolulu, HI, USA, 2022, pp. 141–146. DOI. 10.1109/ICSA-C54293.2022.00035.
- [12] S. Hadfield, Z. Wang, B. O’Gorman, E. G. Rieffel, D. Venturelli, and R. Biswas, “From the quantum approximate optimization algorithm to a quantum alternating operator ansatz,” *Algorithms*, vol. 12, no. 2, pp. 34, Feb. 2019, DOI. 10.3390/a12020034.
- [13] Z. Wang, N. C. Rubin, J. M. Dominy, and E. G. Rieffel, “XY mixers: analytical and numerical results for the quantum alternating operator ansatz,” *Phys Rev. A*, vol. 101, no. 1, pp. 012320, Jan. 2020, DOI. 10.1103/PhysRevA.101.012320.
- [14] S. Marsh and J. B. Wang, “A quantum walk-assisted approximate algorithm for bounded NP optimisation problems,” *Quantum Information Processing*, vol. 18, pp. 1–18, Jan. 2019, DOI. 10.1007/s11128-019-2171-3.
- [15] A. Bärtschi and S. Eidenbenz, “Grover mixers for QAOA: shifting complexity from mixer design to state preparation,” in *2020 IEEE International Conference on Quantum Computing and Engineering (QCE)*, Denver, CO, USA, 2020, pp. 72–82. DOI. 10.1109/QCE49297.2020.00020.
- [16] Y. Wang, “A quantum approximate Bayesian optimization algorithm for continuous problems,” in *2021 IISE Annual Conference & Expo*, New Orleans, LA, USA, 2021, pp. 235–240.
- [17] L. C. G. Govia, C. Poole, M. Saffman, and H. K. Krovi, “Freedom of the mixer rotation axis improves performance in the quantum approximate

- optimization algorithm,” *Phys Rev. A*, vol. 104, no. 6, pp. 062428, Dec. 2021, DOI. 10.1103/PhysRevA.104.062428.
- [18] Y. Chen, L. Zhu, N. J. Mayhall, E. Barnes, and S. E. Economou, “How much entanglement do quantum optimization algorithms require?” in *Quantum 2.0 Conference 2022*, Boston, MA, USA, 2022, pp. QM4A-2. DOI. 10.1364/QUANTUM.2022.QM4A.2.
- [19] S. Brandhofer *et al.*, “Benchmarking the performance of portfolio optimization with QAOA,” *Quantum Information Processing*, vol. 22, no. 1, pp. 1–27, Dec. 2022, DOI. 10.1007/s11128-022-03766-5.
- [20] P. Niroula *et al.*, “Constrained quantum optimization for extractive summarization on a trapped-ion quantum computer,” *Scientific Reports*, vol. 12, no. 1, pp. 17171, Oct. 2022, DOI. 10.5281/zenodo.6819861.
- [21] R. LaRose, E. Rieffel, and D. Venturelli, “Mixer-phaser ansätze for quantum optimization with hard constraints,” *Quantum Machine Intelligence*, vol. 4, no. 17, Jun. 2022, DOI. 10.1007/s42484-022-00085-x.
- [22] L. K. Grover, “A fast quantum mechanical algorithm for database search,” in *STOC '96: Proc. of the Twenty-Eighth Annual ACM Symposium on Theory of Computing*, Philadelphia, PA, USA, 1996, pp. 212–219. DOI. 10.1145/237814.237866.
- [23] Y. Yu, C. Cao, C. Dewey, X. B. Wang, N. Shannon, and R. Joynt, “Quantum approximate optimization algorithm with adaptive bias fields,” *Phys. Rev. Research*, vol. 4, no. 2, pp. 023249, Jun. 2022, DOI. 10.1103/PhysRevResearch.4.023249.
- [24] N. Chancellor, “Domain wall encoding of discrete variables for quantum annealing and QAOA,” *Quantum Science and Technology*, vol. 4, no. 4, pp. 045004, Aug. 2019, DOI. 10.1088/2058-9565/ab33c2.
- [25] C. Xue, Z. Y. Chen, Y. C. Wu, and G. P. Guo, “Effects of quantum noise on quantum approximate optimization algorithm,” *Chinese Physics Letters*, vol. 38, no. 3, pp. 030302, Mar. 2021, DOI. 10.1088/0256-307X/38/3/030302.
- [26] J. Marshall, F. Wudarski, S. Hadfield, and T. Hogg, “Characterizing local noise in QAOA circuits,” *IOP SciNotes*, vol. 1, no. 2, pp. 025208, Aug. 2020, DOI. 10.1088/2633-1357/abb0d7.
- [27] J. Roffe, “Quantum error correction: an introductory guide,” *Contemporary Physics*, vol. 60, no. 3, pp. 226–245, Oct. 2019, DOI. 10.1080/00107514.2019.1667078.
- [28] P. W. Shor, “Scheme for reducing decoherence in quantum computer memory,” *Phys. Rev. A*, vol. 52, no. 4, pp. R2493, Oct. 1995, DOI. 10.1103/PhysRevA.52.R2493.

- [29] D. Gottesman, “Stabilizer codes and quantum error correction,” Ph.D. dissertation, Dept. Physics, California Institute of Technology, Pasadena, CA, USA, 1997.
- [30] A. Y. Kitaev, “Fault-tolerant quantum computation by anyons,” *Annals of Physics*, vol. 303, no. 1, pp. 2–30, Jan. 2003, DOI. 10.1016/S0003-4916(02)00018-0.
- [31] E. Dennis, A. Kitaev, A. Landahl, and J. Preskill, “Topological quantum memory,” *Journal of Mathematical Physics*, vol. 43, no. 9, pp. 4452–4505, Aug, 2002, DOI. 10.1063/1.1499754.
- [32] W. Cai, Y. Ma, W. Wang, C. L. Zou, and L. Sun, “Bosonic quantum error correction codes in superconducting quantum circuits,” *Fundamental Research*, vol. 1, no. 1, pp. 50–67, Jan, 2021, DOI. 10.1016/j.fmre.2020.12.006.
- [33] J. Müller, W. Lavrijsen, C. Iancu, and W. de Jong, “Accelerating noisy VQE optimization with Gaussian processes,” in *2022 IEEE International Conference on Quantum Computing and Engineering (QCE)*, Broomfield, CO, USA, 2022, pp. 215–225, DOI. 10.1109/QCE53715.2022.00041.
- [34] A. Gilliam, S. Woerner, and C. Gonciulea, “Grover adaptive search for constrained polynomial binary optimization,” *Quantum*, vol. 5, pp. 428, Apr. 2021, DOI. 10.22331/q-2021-04-08-428.
- [35] A. Perdomo-Ortiz, N. Dickson, M. Drew-Brook, G. Rose, and A. Aspuru-Guzik, “Finding low-energy conformations of lattice protein models by quantum annealing,” *Scientific Reports*, vol. 2, no. 1, pp. 1–7, Aug. 2012, DOI. 10.1038/srep00571.
- [36] K. Setia, R. Chen, J. E. Rice, A. Mezzacapo, M. Pistoia, and J. D. Whitfield, “Reducing qubit requirements for quantum simulations using molecular point group symmetries,” *Journal of Chemical Theory and Computation*, vol. 16, no. 10, pp. 6091–6097, Aug. 2020, DOI. 10.1021/acs.jctc.0c00113.
- [37] A. Tran, M. Tran, and Y. Wang. "Constrained mixed-integer Gaussian mixture Bayesian optimization and its applications in designing fractal and auxetic metamaterials," *Structural and Multidisciplinary Optimization*, vol. 59, pp. 2131–2154, Jan. 2019, DOI. 10.1007/s00158-018-2182-1.
- [38] D. Datta and J. R. Figueira, “A real-integer-discrete-coded particle swarm optimization for design problems,” *Applied Soft Computing*, vol. 11, no. 4, pp. 3625–3633, Jun. 2011, DOI. 10.1016/j.asoc.2011.01.034.
- [39] L. C. Cagnina, S. C. Esquivel, and C. A. C. Coello, “Solving engineering optimization problems with the simple constrained particle swarm optimizer,” *Informatica*, vol. 32, no. 3, pp. 319–326, Jan. 2008.